EXTENDING THE HUMAN FOVEAL SPATIAL CONTRAST SENSITIVITY FUNCTION TO HIGH LUMINANCE RANGE

Christos Kaspiris-Rousellis, Maydel Fernandez-Alonso and Jenny C. A. Read

Institute of Neuroscience, Newcastle University, Tyne and Wear, UK

ABSTRACT

The human contrast sensitivity function (CSF) is the most general way of quantifying what human vision can perceive. It predicts which artifacts will be visible on a display and what changes to hardware will result in noticeable improvements. Contrast sensitivity varies with luminance, and as new technology is producing higher luminance range displays, it is becoming essential to understand how the CSF behaves in this regime. Following this direction, we investigated the effect of adaptation luminance on contrast sensitivity for sine-wave gratings over a large number of CSF measurements in the literature. We examined the validity of the linear to DeVries-Rose to Weber region transition that is usually assumed to predict this relationship. We found a gradual transition among the three regions with steeper/flatter slopes for higher/lower frequencies and lower/higher retinal illuminance. A further decreasing region was located at low to intermediate frequencies, which was consistent across studies. Based on this theoretical construct, we adopted a CSF model consisting of central elements in the human visual signal processing and three limiting internal noise components corresponding to each region. We assessed the model's performance on the measured contrast sensitivities and proposed an eight-parameter form to describe the contrast sensitivity surface in the spatial frequency-luminance domain.

Index Terms — adaptation luminance, CSF, DeVries-Rose, sine-wave gratings, spatial resolution, visual system, Weber

1. INTRODUCTION

The most basic way of characterizing the ability of a human observer to discriminate visual patterns is the contrast sensitivity function (CSF). The CSF reports the sensitivity to visual stimuli as a function of their spatiotemporal frequency. It is an integral part of visual display standardization (e.g., [1]), and the central component in HVS-based image quality assessment algorithms for extending performance to higher luminance range (e.g., [2, 3]). The latter stems from the fact that one of the primary factors determining the shape of the CSF is adaptation luminance. Generally, an increase in the mean background luminance results in higher peak sensitivity and spatial resolution, while the location of the peak shifts to higher frequencies, additionally changing the CSF shape from low-pass to band-pass [4, 5, 6, 7, 8].

The relationship between contrast sensitivity and adaptation luminance is often described as a trilinear transition [8, 9] with each segment corresponding to the dominant noise source that limits visual detection, i.e., early noise or "dark light" [10], photon shot noise [11, 12], and late neural noise [13]. This theoretical construct is usually referred to as linear to DeVries-Rose to Weber transition, with slopes equal to 1, 0.5, and 0 in log-log space for each segment, respectively. In the case of sine-wave gratings, employed in CSF measurements, sensitivity was found to demonstrate asymptotic behavior (i.e., to approach the Weber region) at higher luminance for increasing spatial frequency [5, 14, 15]. Several studies provide evidence for a further decreasing, albeit neglected, region for low to intermediate ($\sim$ 8 cpd) spatial frequencies [7, 8, 16, 17, 18, 19, 20, 21, 22, 23]. This interesting phenomenon of a decrease in sensitivity with increasing luminance was briefly discussed in [24, 25].

The suitability of this construct for describing sine-wave contrast sensitivity as a function of luminance intensity has been questioned over the years [24, 26]. Although this approach constitutes a simplified model of a complex system of contributing adaptation mechanisms, e.g., different types of photoreceptors and their interactions, it has been proven successful in approximating sensitivity variations in the luminance domain [8, 13, 27] and forms the basis of the most widely-used class of CSF models [15, 28].

Here, we assess this non-linear relationship on a wide range of studies in the literature [4, 5, 7, 8, 14, 15, 16, 20, 21, 22, 23, 29, 30, 31, 32, 33] using continuous piecewise linear regression analysis. This regression method is structured to answer whether for a given luminance range: (a) sensitivity is independent of luminance (i.e., a single segment with zero slope), (b) a critical point of change in the slope exists, (c) the linear to DeVries-Rose to Weber law holds (i.e., transition from a slope of 1 to 0.5 to 0), and (d) a decreasing region is present (i.e., a segment with negative slope). We then adopt a variant of the models derived from this construct [15] that incorporates basic elements in the human visual signal processing to describe the CSF in the luminance domain. It comprises optical factors, the addition of photon shot noise, lateral inhibition, the addition of late neural noise, and a matched filter [34] with a sampling aperture. The model (Figure 1) was adjusted to include an additional early neural noise component (related to the linear segment preceding the DeVries-Rose region) that was found to dominate low luminance intensities and spatial frequencies [8]. Finally, we examine the model's performance on the measured CSFs and evaluate the basic CSF characteristics as a function of luminance, namely, the location and amplitude of the peak, the area under the curve, and the spatial resolution limit.

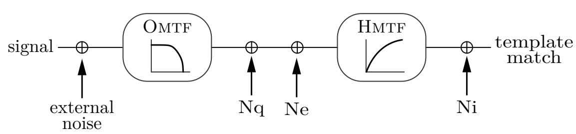

Figure 1. Block diagram of the visual processing model. The stimulus is low-pass filtered by the optical modulation transfer function (O_{MTF}) of the eye before photon (N_q) and early noise (N_e) components are added. A high-pass filter (H_{MTF}) is then applied due to lateral inhibition, and late internal noise is added (N_i) before the signal is interpreted. External noise is included for completeness but assumed negligible in this study.

The work in this paper was funded from the European Union's Horizon 2020 research and innovation program under the Marie Skłodowska-Curie grant agreement No 676401, European Training Network on Full Parallax Imaging.

2. METHODS

2.1. Pre-processing

Unavailable data were extracted from the published figures using the software in [35]. Retinal illuminance values were corrected for the Stiles-Crawford effect [36] following the equation in [37] with a β co-efficient of 0.12 [38]. The same formula was used to convert display luminance values to retinal illuminance. Where unavailable, pupil size was approximated for the corresponding adaptation luminance using the unified formula in [39] for an observer of twenty-five years old or the study population mean.

2.2. Segmented regression

Breakpoints were estimated using the iterative method described in [40]. Given one breakpoint the model is expressed as:

$$S_i = \alpha + \beta_1 I + U_1 (I - \psi_1)_+ \tag{1}$$

where $(I - \psi_1)_+ = (I - \psi_1) \times G(I > \psi_1)$ and $G(\cdot)$ is a step function equal to one when $I > \psi_1$ and zero otherwise, S_i denotes the sensitivity for a spatial frequency u_i, I the retinal illuminance, α is the intercept, β_1 is the slope of the segment before the breakpoint ψ_1, and $\beta_2 = U_1 + \beta_1$ is the slope of the segment after the breakpoint. Additional breakpoints can be estimated similarly by adding the appropriate terms to equation (1).

The existence of a breakpoint, i.e., the null hypothesis of a zero change in slope, was validated using a two-sided Davies test [41] at 0.05 significance level with the additional constraint of its confidence interval to lie within the measured luminance boundaries. For the breakpoint estimation, the number of points was increased by N-1, where N is the total number of samples, using a shape-preserving piecewise cubic interpolation [42] on the midpoints between each pair of luminance values.

2.3. Extending the CSF to the luminance domain

Following the model derived in [15, 25], with the assumption that critical illuminance is independent of grating stimulus area and external noise is negligible, the sensitivity-illuminance curve for spatial frequency u_i can be described by:

$$S(u_i, I) = S'_{\max}(u_i) \left[1 + \frac{I_{c_i}}{I} + \left(\frac{I_{d_i}}{I} \right)^2 \right]^{-0.5} \tag{2}$$

where S is the Michelson contrast sensitivity, $S'_{\max}$ the sensitivity ceiling for a constant grating area, I the retinal illuminance, and I_{d_i} and I_{c_i} the frequency-dependent critical illuminances that mark the transition from the linear to DeVries-Rose and DeVries-Rose to Weber regions, respectively. It should be noted that this form implies a gradual transition, that is qualitatively in better agreement with experimental findings [25] and satisfies the empirical constraints in [26]. The $S'_{\max}$ is defined as:

$$S'_{\max}(u_i) = S_{max}(u_i) \left[1 + \left(\frac{A_c(u_i)}{A} \right)^{-0.5} \right] \tag{3}$$

where A is the stimulus grating area and $A_c(u_i)$ the critical area where spatial integration saturates. Assuming that the latter is independent of retinal illuminance, it can be expressed as:

$$A_c(u_i) = A_0 \left[1 + \left(\frac{u_i}{u_{max}} \right)^2 \right]^{-1} \tag{4}$$

where A_0 and u_{max} the upper spatial summation limits for the grating area and the critical spatial frequency, respectively. The S_{max} is then given as:

$$S_{max}(u_i) = K_0 O_{MTF}(u_i) H_{MTF}(u_i) \sqrt{A_c(u_i)} \tag{5}$$

where K_0 is a constant, O_{MTF} is the low-pass optical modulation transfer function, and H_{MTF} is the high-pass filter due to lateral inhibition. The constant K_0 is expressed as:

$$K_0 = \sqrt{\frac{\eta_{max}}{2d'^2 N_i}} \tag{6}$$

where η_{max} is the maximum efficiency of the local matched filter, d' is a detectability constant [43] that depends on the task and the threshold level, and N_i is the late noise. The choice of the human optical MTF formula varies in the literature [44]. Here, for comparison purposes, we adopt a Gaussian form [28] that accounts for both the optical attenuation and retinal sampling factors:

$$O_{MTF}(u_i) = e^{-2\pi^2 \sigma(d)^2 u_i^2} \tag{7}$$

where $\sigma(d)$ is the standard deviation of the line-spread function as a function of pupil diameter d [mm]:

$$\sigma(d) = \sqrt{\sigma_0^2 + (C_{ab} d)^2} \tag{8}$$

where σ_0 can be considered constant for foveal vision and C_{ab} an increment weight for increasing pupil size estimated at 0.08 arcmin/mm [28]. In the original model, low-frequency attenuation was found to decrease linearly with increasing spatial frequency. However, this appears to be valid only at a limited frequency range [45]. Here, we adopt the following approximation formula for lateral inhibition [28] but allowing for the square exponent to vary:

$$H_{MTF}(u_i) = \sqrt{1 - e^{-(u_i/u_0)^\nu}} \tag{9}$$

where u_0 is the upper frequency limit for lateral inhibition and ν is a free parameter.

The best fit for the parameters K_0, u_0, σ_0, κ, and the vectors $\mathbf{I}_c$ and $\mathbf{I}_d$ was found by simultaneously minimizing the sum of errors in log-space for all spatial frequencies with more than two samples in luminance. Where the total number of frequencies was below four, the sensitivity-illuminance curves were estimated using equation (2) with $\mathbf{S}'_{\max}$ as a free parameter. The summation parameters A_0 and u_{max} were fixed at 320 deg^2 and 0.465 c/deg, respectively, as estimated in [15]. Although the actual values might differ, any deviation will be reflected in the variability of the fitted parameters among studies. Fitting performance is expressed as the root mean square (RMS) and normalized root mean square (NRMS) errors, as defined in [46]. The normalization was used to correct for the number of free parameters.

3. RESULTS

Figure 2 illustrates the model fit to the measured contrast sensitivities as a function of retinal illuminance for all spatial frequencies across studies. Where applicable, the model was fitted to the average observer (eleven studies). Despite the vast differences in the experimental conditions, the data exhibit a qualitatively similar relationship to the background luminance. Generally, as the spatial frequency increases, the curve becomes steeper, and the asymptotic region translates to higher luminance. The RMS error for each study is shown at the top left of each panel in Figure 2. The total RMS error for all studies combined was 1.19dB.

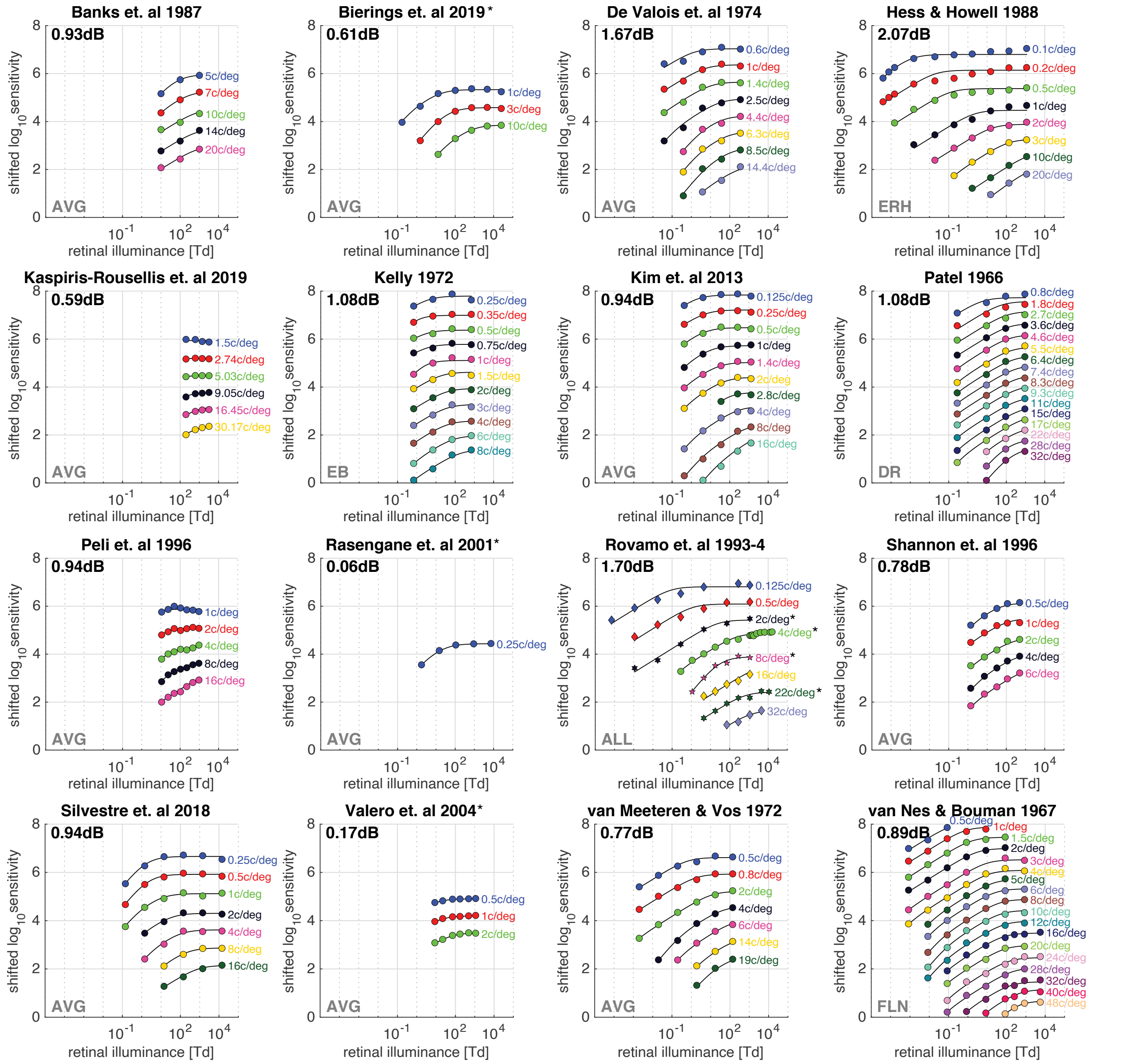

Figure 2. The model fit (black lines) to the measured sensitivity data (markers $\approx 0.25 \log_{10}$ units width) for each spatial frequency [c/deg] as a function of retinal illuminance [Td] across studies. Different markers indicate different observers. Sensitivities were vertically shifted from higher to lower spatial frequency for visualization purposes. The RMS error [dB] is shown at the top left of each panel. The observers' initials are shown at the bottom left, where 'AVG' and 'ALL' indicate the average and all the observers, respectively. The asterisk indicates a model fit with S'_{max} as a free parameter.

Figure 3 summarizes the results of the segmented regression analysis on the measured contrast sensitivity data. For visualization purposes, the slopes of each segment are presented as a function of relative retinal illuminance, i.e., the retinal illuminance divided by the spatial frequency squared [27]. Qualitatively, a region where the DeVries-Rose to Weber law holds in a strict sense (an arbitrary threshold of ±0.05 difference from the predicted slopes of 0.5 and 0) does seem to exist for specific luminance and frequency conditions, but generally, this range seems restricted (see dashed thin lines in Figure 3, panels A2-3, C2, and C4-5). Instead, the slopes gradually decrease with increasing relative illuminance from a value between 0.5 and 1 to zero approaching a Weber region. This observation translates as follows: For decreasing/increasing retinal illuminance or increasing/decreasing frequency, the transition towards the contrast sensitivity ceiling becomes steeper/more flat. Negative-slope segments, below an arbitrary threshold value of -0.1 (M = -0.19, SD = 0.09), were found in four of the studies [15, 18, 20, 23] at spatial frequencies between 0.25 cpd and 8 cpd and starting log relative illuminance between 0.79 and 3.20 Td deg^2. A negative slope was also present in [5, 7, 8, 14, 16, 21, 33] at roughly the same frequency range that can, however, be considered as negligible (M = -0.05, SD = 0.02). It should be noted that in two of the studies [31, 32] the stimuli were temporally modulated at a low temporal frequency (6 Hz) that could diverge the slope values from the ideal DeVries-Rose to Weber transition depending on luminance [18]. However, in both cases, the slopes were in relatively better agreement with this law compared to the rest of the data.

The fitted global parameter values are given in Table 1. The mean estimates were K_0 = 345 (SD = 236), u_0 = 5.5 (SD = 3.6) c/deg, σ_0 = 0.5 (SD = 0.1) arcmin, and ν = 2.4 (SD = 0.6). Estimates near the parameter boundaries were excluded. A possible explanation for this discrepancy is discussed below. In another variant of the same class of models, the one from Barten [28],

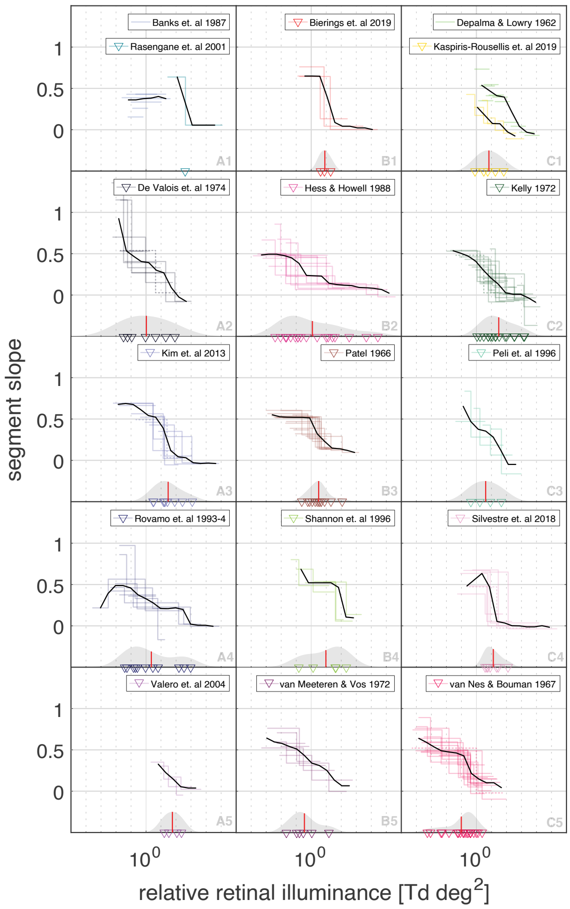

Figure 3. The segmented regression slopes across studies as a function of relative retinal illuminance [Td deg^2]. The thin lines depict the slope of the segments for each spatial frequency. The dashed thin lines indicate a transition with slopes 0.50±0.05 and ±0.05. The thick black curves show the median slope over a non-overlapping sliding window of 0.5 log units. The markers depict the estimated breakpoints and the vertical red lines the mean value of their density estimate. The studies in panels A1 and A3 were grouped for visualization purposes.

u_0, and σ_0 were estimated at 7 c/deg and 0.5 arcmin, respectively, while the parameter ν was assumed fixed at 2. The estimated critical illuminance vectors are presented in Figure 4. The critical illuminance I_c that marks the transition to a Weber region was found to be log-linearly related to spatial frequency, over a wide frequency range. Previous studies indicated that I_c is approximately proportional to the spatial frequency squared [5, 15, 27], i.e., a slope of 2. We estimated a mean slope of 1.7 (SD = 0.6), in good agreement with the above. The relation between the spatial frequency and the critical quantity I_d was less clear, mainly since the luminance-frequency sampling across studies did not allow for reliable estimates. However, at this point, we will assume a first-degree polynomial approximation. Therefore the parameters I_c and I_d as a function of frequency can be expressed as:

$$log_{10} I_c(u) \approx \text{constant}_c + \text{slope}_c \, log_{10} u \tag{10}$$

$$log_{10} I_d(u) \approx \text{constant}_d + \text{slope}_d \, log_{10} u \tag{11}$$

Based on the above results, we explored the effect of reducing the critical illuminance parameters on the total RMS error for all the studies combined. This is an essential step as it not only considerably reduces the total estimated parameters, but it also allows us to extract the CSF surface in the frequency-luminance do-

Table 1. The estimated global parameters. In the parenthesis, the observer's initials, where 'AVG' the average observer. A value of 'UB' indicates the upper bound (set at 16 cpd), and the gray color a fixed value.

Study	K_0	u_0 [c/deg]	σ_0 [arcmin]	ν
Banks et. al 1987 (AVG)	107.45	2.98	0.37	2.00
De Valois et. al 1974 (AVG)	145.10	3.67	<0.1	2.91
Hess & Howell 1988 (ERH)	843.90	13.64	0.50	2.33
Kaspiris-Rousellis et. al 2019 (AVG)	409.18	3.45	0.68	2.75
Kelly 1972 (EB)	137.79	1.66	<0.1	3.92
Kim et. al 2013 (AVG)	237.14	3.45	<0.1	2.03
Patel 1966 (DR)	634.84	UB	0.53	2.24
Peli et. al 1996 (AVG)	76.03	2.38	0.41	2.54
Rovamo et. al 1994 (JM)	375.23	7.54	<0.1	1.95
Shannon et. al 1996 (AVG)	253.80	UB	<0.1	1.30
Silvestre et. al 2018 (AVG)	177.36	3.54	<0.1	2.58
van Meeteren & Vos 1972 (AVG)	389.49	7.39	0.74	2.30
van Nes & Bouman 1967 (FLN)	699.34	10.45	0.36	2.42

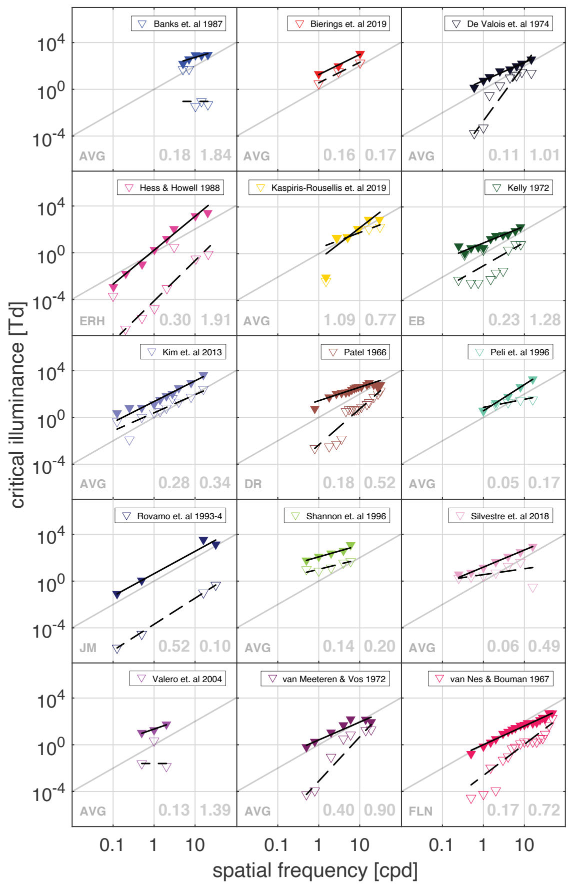

Figure 4. The critical illuminance vectors I_c (filled symbols) and I_d (open symbols) as a function of spatial frequency. The grey line illustrates a critical illuminance proportional to the spatial frequency squared. The solid and the dotted lines depict the log-linear regressions for the I_c and I_d vectors, respectively. On the bottom left the observer's initials, where 'AVG' indicates the average observer. On the bottom right, the RMS errors in log units left for I_c and right for I_d.

main. If we fixed slope$_c$ = 2 in equation (10), and fitted constant$_c$ along with the individual values of $\mathbf{I}_d$, the RMS and NRMS error increased by 1.31dB and 1.37dB, respectively. Fitting slope$_c$ as well, resulted in a smaller increase of 0.53dB and 0.45dB in RMS and NRMS errors, respectively. Fitting all four terms in equations (10) and (11) led to an increase of 1.27dB and 1.07dB for the RMS and NRMS errors, respectively. Increasing the polynomial terms further did not produce any considerable improvement.

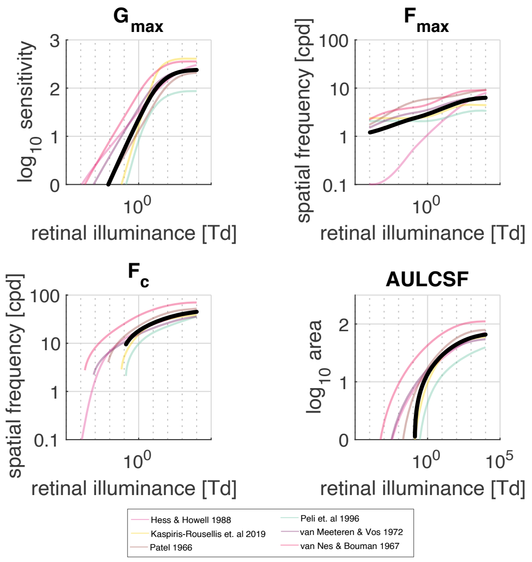

Figure 5. The main CSF characteristics as a function of retinal illuminance. Top left: The peak sensitivity. Top right: The spatial frequency of the peak. Bottom left: The high-frequency cut-off where sensitivity asymptotes to zero. Bottom right: The area under the log-CSF. The thin lines depict different studies. The thick black line is the mean.

In Figure 5 we examine the relationship of the main CSF characteristics to retinal illuminance across studies, namely, the location (F_{max}) and the magnitude (G_{max}) of peak sensitivity, the high-frequency cut-off (F_c) where sensitivity asymptotes to zero, and the area under the log-CSF (AULCSF). The grating area was kept constant at 4 deg^2. Where the pupil size was not fixed, it was estimated as described in the methods section. Datasets with limited sampling in spatial frequency or estimates of the optical attenuation factor σ_0 near the boundary were excluded from further analysis. The peak sensitivity was predicted to asymptote above roughly 10^3 Td, while the peak frequency gradually increased from about 1 to 10 cpd with increasing illuminance. It should be noted that the predicted relationship for the high-frequency cut-off (i.e., visual acuity) does not account for a well-known discontinuity [26, 47] during the transition from scotopic to photopic conditions ($\approx$ between 4.7×10^{-3} and 710 Td) [48].

4. DISCUSSION

In this study, we analyzed foveal contrast sensitivity measurements in the literature that systematically investigated the effect of different background luminance levels on the CSF. We focused on a theoretical construct that describes this relationship, the linear to DeVries-Rose to Weber transition, which manifests as an increase in sensitivity with increasing luminance with slopes of 1 and 0.5 in double log space to a Weber region where sensitivity becomes independent of luminance (i.e., a slope of zero). By using continuous segmented regression analysis, we found that the DeVries-Rose to Weber transition in a strict sense holds only for a limited range across spatial frequencies and luminance conditions. Instead, a curvilinear form with a gradual transition among the three regions appears as a valid approximation for sine-wave gratings. Specifically, when relative retinal illuminance decreased, either by increasing the spatial frequency or decreasing the retinal illuminance, the transition towards the sensitivity ceiling became steeper, in agreement with the empirical constraints derived in [26]. Except for one study [5], there was insufficient evidence for a Weber region beyond approximately 16 cpd, i.e., increasing luminance continues to increase log sensitivity, and no saturation occurs at the luminance range tested (up to $\approx 10^4$ Td). A decrease in sensitivity with increasing luminance was present at frequencies between 0.25 cpd and 8 cpd for a large number of studies (Figure 3, panels A2-5, and C1-5). However, the slope of decrease was relatively small, and the results do not suffice to draw any further conclusions. It should be noted, though, that in most cases, we used the average observer that could cancel out any related individual differences [24].

Table 2. The fitted constants in the approximation of I_c and I_d. In the parenthesis the observer's initials, where 'AVG' the average observer.

Study	constant$_c$	slope$_c$	constant$_d$	slope$_d$
Banks et. al 1987 (AVG)	1.48	1.20	-0.10	0
Bierings et. al 2019 (AVG)	1.24	1.72	0.55	1.75
De Valois et. al 1974 (AVG)	0.80	1.50	-2.18	3.97
Hess & Howell 1988 (ERH)	0.31	3.08	-3.32	2.71
Kaspiris-Rousellis et. al 2019 (AVG)	-1.17	3.21	0.91	0.97
Kelly 1972 (EB)	0.82	1.58	-1.23	1.68
Kim et. al 2013 (AVG)	1.47	1.55	0.41	1.60
Patel 1966 (DR)	1.64	0.88	-1.99	2.84
Peli et. al 1996 (AVG)	0.57	2.24	0.73	0.76
Rovamo et. al 1994 (JM)	0.68	1.93	-3.75	2.27
Shannon et. al 1996 (AVG)	2.08	1.11	1.04	0.75
Silvestre et. al 2018 (AVG)	1.17	1.48	0.64	0.94
Valero et. al 2004 (AVG)	1.34	1.20	-1.03	0
van Meeteren & Vos 1972 (AVG)	0.50	1.51	-2.79	3.83
van Nes & Bouman 1967 (FLN)	-0.02	1.64	-3.24	3.07

Following this construct, we adopted a model [15] consisting of a low-pass optical MTF, a high-pass MTF due to lateral inhibition, a local matched filter, and two noise sources (photon shot noise and late proximal noise) that limit visual detection across the luminance domain and generate this observed DeVries-Rose to Weber transition. We modified the model to include an additional early noise component that relates to the linear to DeVries-Rose transition (I_d) and was found to have a significant effect at low luminance and spatial frequencies [8]. The preliminary segmented regression analysis revealed slopes between 1 and 0.5 that further supports the existence of a third region, in the context of this model, where contrast sensitivity becomes proportional to the background luminance. The critical illuminance that marks the transition to a Weber region was found to be log-linearly related to the spatial frequency, consistent with the above results. It was roughly proportional to spatial frequency squared, a phenomenon that is usually explained neurophysiologically by the constant-flux hypothesis [9, 27]. Our proposed model with eight parameters, i.e., equations (2) - (11) resulted in a total RMS error of 2.46dB for all the studies combined, but further improvements can be made. The estimated constants in equations (10) and (11) for approximating the critical quantities I_c and I_d are given in Table 2.

Scrutiny of the global parameters among studies revealed an inconsistency in the estimation of σ_0, which controls the optical attenuation at high spatial frequencies. This discrepancy could be an artifact due to limited frequency range sampling [18, 31], or an overestimation of the pupil diameter. Except for one of these studies, pupil size was estimated from the display luminance [7, 21], or it was artificially dilated to a high value [15]. In two of the studies, the parameter u_0, the spatial frequency where the low-frequency attenuation ceases, was at the upper boundary. A possible explanation would be the presence of a local notch on the CSF [4], and limited frequency range sampling as above [31]. The variability in the estimation of the constant K_0 was expected due to the vast differences in the experimental conditions. Nevertheless, fixing these parameters still provided us with reasonable fits.

However, other factors might be present. In the derivation of the model, we assumed that the critical area where spatial summation saturates is independent of retinal illuminance. A violation of this assumption would also cause this discrepancy. In fact, in an extension of a similar model variant, the one by Barten [28], to scotopic conditions [49], the spatial integration along with other parameters were adjusted to eccentric viewing that is more appropriate for rod-dominated vision. This approach essentially assumes a discontinuous piecewise function in luminance for the otherwise fixed model parameters, that was found successful in describing contrast sensitivity measurements under scotopic (i.e., rod-dominated) conditions. Inspecting the prediction of our model variant on the main CSF characteristics revealed a limitation at low light levels, i.e., no discontinuity in acuity during the transition from the scotopic to the photopic range, that constrains its application to moderate or higher light levels and foveal vision. A similar two-segment relationship could be investigated here.

Another drawback of this modeling approach is that it does not account for any decrease in sensitivity with increasing luminance, and therefore it is also upper-bounded for low to intermediate frequencies. Incorporating a decreasing term in equation (2) is trivial (e.g., by adding the term $(I/I_b)^b$ in the parenthesis, where I_b the transition point and b the slope of decrease). However, this does not appear to be theoretically justified, and high-luminance data where this could be more accurately examined are scarce.

Alternatively, given sufficiently dense sampling in luminance and frequencies, it is feasible to extend the CSF only by interpolating the parameters of a mathematical form (e.g., an asymmetric log-parabola [50]) in the luminance domain. An advantage of this approach is that by definition it can describe the decreasing sensitivity at lower frequencies while there is still sensitivity increase at the high-end with increasing luminance, and thus can be extended to high light levels and different conditions where this decrease is prominent (e.g., peripheral stimuli [17]). This technique also allows for capturing other CSF features (e.g., low-frequency truncation [46]). However, this approach is highly sensitive to measurement noise. We found that combining our model variant for interpolating across luminance with an asymmetric log-parabola form for interpolating across spatial frequencies performed similarly with the same number of free parameters, but could lead to an overestimation of the spatial resolution limit.

Whereas a modeling approach incorporating elements from the neurophysiology of vision (e.g., photoreceptor responses, retinal gain controls) would provide a more accurate description, this much more straightforward approach is a reasonable approximation to psychophysically and electrophysiologically [31] measured contrast sensitivity variations in the luminance domain and allows for the extraction of the CSF surface as a function of light level over a wide range of normal viewing conditions.

5. REFERENCES

[1] NEMA PS 3.14, Digital Imaging and Communications in Medicine (DICOM) Standard, Part 14: Grayscale Standard Display Function, National Electrical Manufacturers Association, Rosslyn, VA, USA. (page 1)

[2] S. J. Daly, “Visible differences predictor: an algorithm for the assessment of image fidelity,” in *Human Vision, Visual Processing, and Digital Display III* (B. E. Rogowitz, ed.), vol. 1666, p. 2, 1992. (page 1)

[3] R. Mantiuk, K. J. Kim, A. G. Rempel, and W. Heidrich, “HDR-VDP-2,” in *ACM SIGGRAPH 2011 papers on - SIGGRAPH ’11*, (New York, New York, USA), p. 1, ACM Press, 2011. (page 1)

[4] A. S. Patel, “Spatial Resolution by the Human Visual System The Effect of Mean Retinal Illuminance*,” *Journal of the Optical Society of America*, vol. 56, no. 5, p. 689, 1966. (page 1, 5)

[5] F. L. Van Nes and M. A. Bouman, “Spatial Modulation Transfer in the Human Eye,” *Journal of the Optical Society of America*, vol. 57, no. 3, p. 401, 1967. (page 1, 3, 4, 5)

[6] A. van Meeteren and J. Vos, “Resolution and contrast sensitivity at low luminances,” *Vision Research*, vol. 12, no. 5, pp. 825–IN2, 1972. (page 1)

[7] R. L. De Valois, H. Morgan, and D. M. Snodderly, “Psychophysical studies of monkey Vision-III. Spatial luminance contrast sensitivity tests of macaque and human observers,” *Vision Research*, vol. 14, no. 1, pp. 75–81, 1974. (page 1, 3, 5)

[8] D. Silvestre, A. Arleo, and R. Allard, “Internal noise sources limiting contrast sensitivity.,” *Scientific reports*, vol. 8, no. 1, p. 2596, 2018. (page 1, 3, 5)

[9] N. Van Surdam Graham, *Visual Pattern Analyzers*. Oxford Psychology Series, OUP USA, 2001. (page 1, 5)

[10] H. Barlow, “The physical limits of visual discrimination,” in *Photophysiology*, pp. 163–202, Elsevier, 1964. (page 1)

[11] A. Rose, “The relative sensitivities of television pickup tubes, photographic film, and the human eye,” *Proceedings of the IRE*, vol. 30, no. 6, pp. 293–300, 1942. (page 1)

[12] H. de Vries, “The quantum character of light and its bearing upon threshold of vision, the differential sensitivity and visual acuity of the eye,” *Physica*, vol. 10, no. 7, pp. 553 – 564, 1943. (page 1)

[13] D. Pelli, *The quantum efficiency of vision*, pp. 3–24. Cambridge University Press, 1990. (page 1)

[14] R. Hess and E. Howell, “Detection of low spatial frequencies: A single filter or multiple filters?,” *Ophthalmic and Physiological Optics*, vol. 8, no. 4, pp. 378–385, 1988. (page 1, 3)

[15] J. Rovamo, J. Mustonen, and R. Näsänen, “Modelling contrast sensitivity as a function of retinal illuminance and grating area,” *Vision Research*, vol. 34, no. 10, pp. 1301–1314, 1994. (page 1, 2, 3, 4, 5)

[16] J. J. Depalma and E. M. Lowry, “Sine-Wave Response of the Visual System II Sine-Wave and Square-Wave Contrast Sensitivity*†,” *Journal of the Optical Society of America*, vol. 52, no. 3, p. 328, 1962. (page 1, 3)

[17] J. Daitch and D. Green, “Contrast sensitivity of the human peripheral retina,” *Vision Research*, vol. 9, no. 8, pp. 947–952, 1969. (page 1, 6)

[18] D. Kelly, “Adaptation effects on spatio-temporal sine-wave thresholds,” *Vision Research*, vol. 12, no. 1, pp. 89–IN1, 1972. (page 1, 3, 5)

[19] J. Rovamo, J. Mustonen, and R. Näsänen, “Neural modulation transfer function of the human visual system at various eccentricities,” *Vision Research*, vol. 35, no. 6, pp. 767–774, 1995. (page 1)

[20] E. Peli, L. Arend, and A. T. Labianca, "Contrast perception across changes in luminance and spatial frequency.," *Journal of the Optical Society of America. A, Optics, image science, and vision*, vol. 13, no. 10, pp. 1953–9, 1996. (page 1, 3)

[21] K. J. Kim, R. Mantiuk, and K. H. Lee, "Measurements of achromatic and chromatic contrast sensitivity functions for an extended range of adaptation luminance," p. 86511A, 2013. (page 1, 3, 5)

[22] R. Bierings, T. Overkempe, C. van Berkel, M. Kuiper, and N. Jansonius, "Spatial contrast sensitivity from star- to sunlight in healthy subjects and patients with glaucoma," *Vision Research*, vol. 158, no. March 2018, pp. 31–39, 2019. (page 1)

[23] C. Kaspiris-Rousellis, M. Fernandez-Alonso, and J. C. A. Read, "Human spatial contrast sensitivity at high luminance," *Unpublished manuscript*, July 2019. (page 1, 3)

[24] M. A. García-Pérez and E. Peli, "The transition from DeVries-Rose to Weber's laws: Comments on Rovamo, Mustonen and Näsänen (1995)," *Vision Research*, vol. 37, no. 18, pp. 2573–2576, 1997. (page 1, 5)

[25] J. Rovamo, R. Näsänen, and J. Mustonen, "Transition from DeVries-Rose to Weber's law: Reply to García-Pérez and Peli (1997)," *Vision Research*, vol. 37, no. 18, pp. 2576–2578, 1997. (page 1, 2)

[26] M. A. García-Pérez, "Is the DeVries-Rose to Weber Transition Empirically Possible with Sine-Wave Gratings?," *The Spanish Journal of Psychology*, vol. 8, no. 2, pp. 113–118, 2005. (page 1, 2, 5)

[27] J. Mustonen, J. Rovamo, and R. Näsänen, "The effects of grating area and spatial frequency on contrast sensitivity as a function of light level," *Vision Research*, vol. 33, no. 15, pp. 2065–2072, 1993. (page 1, 3, 4, 5)

[28] P. G. Barten, *Contrast Sensitivity of the Human Eye and Its Effects on Image Quality*. SPIE, 1999. (page 1, 2, 3, 6)

[29] M. S. Banks, W. S. Geisler, and P. J. Bennett, "The physical limits of grating visibility," *Vision Research*, vol. 27, no. 11, pp. 1915–1924, 1987. (page 1)

[30] J. Rovamo, H. Kukkonen, K. Thppana, and R. Näsänen, "Effects of luminance and exposure time on contrast sensitivity in spatial noise," *Vision Research*, vol. 33, no. 8, pp. 1123–1129, 1993. (page 1)

[31] E. Shannon, A. M. Skoczenski, and M. S. Banks, "Retinal illuminance and contrast sensitivity in human infants," *Vision Research*, vol. 36, no. 1, pp. 67–76, 1996. (page 1, 3, 5, 6)

[32] T. A. Rasengane, J. Palmer, and D. Y. Teller, "Infant light adaptation shows Weber's law at photopic illuminances," *Vision Research*, vol. 41, no. 3, pp. 359–373, 2001. (page 1, 3)

[33] E. M. Valero, J. L. Nieves, J. Hernández-Andrés, and J. A. García, "Changes in contrast thresholds with mean luminance for chromatic and luminance gratings: A reexamination of the transition from the DeVries-Rose to Weber regions," *Color Research & Application*, vol. 29, no. 3, pp. 177–182, 2004. (page 1, 3)

[34] G. Hauske, W. Wolf, and U. Lupp, "Matched filters in human vision," *Biological Cybernetics*, vol. 22, no. 4, pp. 181–188, 1976. (page 1)

[35] A. Rohatgi, "Web plot digitalizer: Html5 based online tool to extract numerical data from plot images. version 4.2.," 2012. (page 2)

[36] W. S. Stiles, B. H. Crawford, and J. H. Parsons, "The luminous efficiency of rays entering the eye pupil at different points," *Proceedings of the Royal Society of London. Series B, Containing Papers of a Biological Character*, vol. 112, no. 778, pp. 428–450, 1933. (page 2)

[37] D. A. Atchison and G. Smith, "Chapter 13 - light level at the retina," in *Optics of the Human Eye* (D. A. Atchison and G. Smith, eds.), pp. 117 – 128, Edinburgh: Butterworth-Heinemann, 2000. (page 2)

[38] R. A. Applegate and V. Lakshminarayanan, "Parametric representation of stiles–crawford functions: normal variation of peak location and directionality," *J. Opt. Soc. Am. A*, vol. 10, no. 7, pp. 1611–1623, 1993. (page 2)

[39] A. B. Watson and J. I. Yellott, "A unified formula for light-adapted pupil size," *Journal of Vision*, vol. 12, no. 10, pp. 12–12, 2012. (page 2)

[40] V. M. R. Muggeo, "Estimating regression models with unknown break-points," *Statistics in Medicine*, vol. 22, no. 19, pp. 3055–3071, 2003. (page 2)

[41] R. B. Davies, "Hypothesis testing when a nuisance parameter is present only under the alternative," *Biometrika*, vol. 74, no. 1, pp. 33–43, 1987. (page 2)

[42] C. B. Moler, *Numerical Computing with Matlab*, ch. 3, pp. 93–116. 2004. (page 2)

[43] W. P. Tanner and T. G. Birdsall, "Definitions of d' and η as Psychophysical Measures," *The Journal of the Acoustical Society of America*, vol. 30, no. 10, pp. 922–928, 1958. (page 2)

[44] A. B. Watson, "A formula for the mean human optical modulation transfer function as a function of pupil size," *Journal of Vision*, vol. 13, p. 18, may 2013. (page 2)

[45] K. Donner and S. Hemilä, "Modelling the spatio-temporal modulation response of ganglion cells with difference-of-Gaussians receptive fields: Relation to photoreceptor response kinetics," *Visual Neuroscience*, vol. 13, no. 1, pp. 173–186, 1996. (page 2)

[46] A. B. Watson and A. J. Ahumada, "A standard model for foveal detection of spatial contrast," *Journal of Vision*, vol. 5, no. 9, p. 6, 2005. (page 2, 6)

[47] C. D. Hendley, "The relation between visual acuity and brightness discrimination," *The Journal of General Physiology*, vol. 31, no. 5, pp. 433–457, 1948. (page 5)

[48] A. J. Zele and D. Cao, "Vision under mesopic and scotopic illumination," *Frontiers in Psychology*, vol. 5, no. JAN, 2015. (page 5)

[49] J. R. Jarvis and C. M. Wathes, "Mechanistic modeling of vertebrate spatial contrast sensitivity and acuity at low luminance.," *Visual neuroscience*, vol. 29, no. 3, pp. 169–81, 2012. (page 6)

[50] S. T. L. Chung and G. E. Legge, "Comparing the shape of contrast sensitivity functions for normal and low vision," *Investigative Ophthalmology and Visual Science*, vol. 57, no. 1, pp. 198–207, 2016. (page 6)